Sentinel-1A - First precise orbit determination results

Peter-Contesse, H.; Jäggi, Adrian; Fernández, JJ; Escobar, D.; Ayuga, F.; Arnold, D; Wermuth, M.; Hackel, S.; Otten, M.; Simons, W.

Important note
To cite this publication, please use the final published version (if applicable).
Please check the document version above.

Sentinel-1A – First precise orbit determination results

H. Peter [a,*], A. Jäggi [b], J. Fernández [c], D. Escobar [c], F. Ayuga [c], D. Arnold [b], M. Wermuth [d],
S. Hackel [d], M. Otten [e], W. Simons [f], P. Visser [f], U. Hugentobler [g], P. Féménias [h]

[a] *PosiTim UG, Seeheim-Jugenheim, Germany*
[b] *Astronomical Institute, University of Bern, Bern, Switzerland*
[c] *GMV AD, Tres Cantos, Spain*
[d] *Deutsches Zentrum für Luft- und Raumfahrt, Oberpfaffenhofen, Germany*
[e] *ESA/ESOC, Darmstadt, Germany*
[f] *Delft University of Technology, Faculty of Aerospace Engineering, Delft, The Netherlands*
[g] *Insitut für Astronomische und Physikalische Geodäsie, Technische Universität München, Munich, Germany*
[h] *ESA/ESRIN, Frascati, Italy*

Abstract

Sentinel-1A is the first satellite of the European Copernicus programme. Equipped with a Synthetic Aperture Radar (SAR) instrument the satellite was launched on April 3, 2014. Operational since October 2014 the satellite delivers valuable data for more than two years. The orbit accuracy requirements are given as 5 cm in 3D. In order to fulfill this stringent requirement the precise orbit determination (POD) is based on the dual-frequency GPS observations delivered by an eight-channel GPS receiver.

The Copernicus POD (CPOD) Service is in charge of providing the orbital and auxiliary products required by the PDGS (Payload Data Ground Segment). External orbit validation is regularly performed by comparing the CPOD Service orbits to orbit solutions provided by POD expert members of the Copernicus POD Quality Working Group (QWG). The orbit comparisons revealed systematic orbit offsets mainly in radial direction (approx. 3 cm). Although no independent observation technique (e.g. DORIS, SLR) is available to validate the GPS-derived orbit solutions, comparisons between the different antenna phase center variations and different reduced-dynamic orbit determination approaches used in the various software packages helped to detect the cause of the systematic offset. An error in the given geometry information about the satellite has been found. After correction of the geometry the orbit validation shows a significant reduction of the radial offset to below 5 mm. The 5 cm orbit accuracy requirement in 3D is fulfilled according to the results of the orbit comparisons between the different orbit solutions from the QWG.
© 2017 COSPAR. Published by Elsevier Ltd. This is an open access article under the CC BY-NC-ND license (http://creativecommons.org/licenses/by-nc-nd/4.0/).

Keywords: Copernicus; Sentinel-1; Precise orbit determination; GPS; Phase center variations; Orbit validation

1. Introduction

"Copernicus, …, is the European Programme for the establishment of a European capacity for Earth Observation".[1] The core of the Copernicus programme (Aschbacher and Milagro-Pérez, 2012) are Earth observation satellites. Dedicated satellites for the specific needs of the programme are the Sentinels. Additionally, Contributing Missions, e.g., national and commercial missions, and in situ sensors provide a large amount of data for Copernicus services.

The Synthetic Aperture Radar (SAR) satellite Sentinel-1A (S-1A, Fletcher et al., 2012; Torres et al., 2012) is the first satellite of the Copernicus programme. It was

---

* Corresponding author.
  E-mail address: heike.peter@positim.com (H. Peter).
[1] http://www.copernicus.eu.

launched on April 3, 2014 from Kourou, French Guiana. After a six-month commissioning phase the satellite was set operational in October 2014. Fig. 1 shows an artist's impression of the satellite. Next to the main instrument, the C-Band SAR, the spacecraft is equipped with three star trackers for attitude determination and two 8-channel Global Positioning System (GPS) units (main and redundant) for precise orbit determination (POD). The requirement for the orbit accuracy is given to be better than 5 cm in 3D in the comparison to external processing facilities (GMES, 2004). The Copernicus POD Service (CPOD Service, Fernández et al., 2014, 2015) is in charge of providing the orbital and auxiliary products needed by the Processing Data Ground Segment (PDGS) of the satellite.

In contrary to Sentinel-3A, GPS is the only POD observation technique available for S-1A. Sentinel-3A was launched in February 2016 and the satellite is additionally equipped with a DORIS (Doppler Orbitography and Radiopositioning Integrated by Satellite) receiver and a Laser Retro Reflector (LRR) for independent orbit validation. In the case of S-1A, the orbit validation may only be based on overlap comparisons and on comparisons of orbits derived from GPS observations. As part of CPOD Service the Copernicus POD Quality Working Group (QWG) regularly delivers independent S-1A orbit solutions generated with different software packages and based on different reduced-dynamic orbit determination (Wu et al., 1991) approaches. These alternative orbit solutions are used to check the quality of the official CPOD orbit solutions for S-1A. First orbit comparisons during the commissioning phase of the mission already led to improvements in the CPOD orbit modelling for S-1A (Peter et al., 2015). NAPEOS (Navigation Package for Earth Orbiting Satellites, Springer et al., 2011), the software used for the CPOD Service, has been updated from IERS 2003 (McCarthy and Petit, 2004) to IERS 2010 Conventions (Petit and Luzum, 2010), leading to more consistency with the QWG solutions. Most of the QWG solutions are already based on IERS 2010 Conventions (see Table 3).

Nevertheless, systematic orbit offsets have still been present between the QWG orbit solutions. Although the same observation technique is used, it is possible to detect inconsistencies in the geometry-based information of the satellite. In the case of MetOp-A equipped with a GPS receiver (Loiselet et al., 2000) only as well (for POD and radio occultations), an inter-agency comparison (Montenbruck et al., 2008) revealed a 3 cm radial orbit difference between the different GPS-derived solutions. The discrepancy was considered as an erroneous information in the vector from CoG (Center of gravity) of the satellite to the GPS antenna reference point (ARP).

For GPS-based POD with an accuracy of few cm it is essential to apply receiver antenna phase center variations (PCVs) in the processing (Jäggi et al., 2009). Ground-calibrated PCVs are available for the GPS antennas used on S-1A (Öhgren et al., 2011). As in the case of other Low Earth Orbiter (LEO) missions such as GRACE (e.g. Jäggi et al., 2009), GOCE (Bock et al., 2011), and Swarm (van den IJssel et al., 2015), however, the application of the ground-calibrated PCVs for S-1A leads to a deterioration of the orbit solutions. Therefore, the PCVs are generated based on the carrier phase observation residuals in an in-flight calibration. A first set of PCVs for the main GPS antenna of S-1A have been generated from the CPOD Service at the beginning of the commissioning phase. Some of the members of the POD QWG generated PCVs by themselves. Applying these different sets of PCVs lead to different results when using one of the different software packages mainly with regard to the radial leveling of the orbits. Investigations on the systematic offsets show that
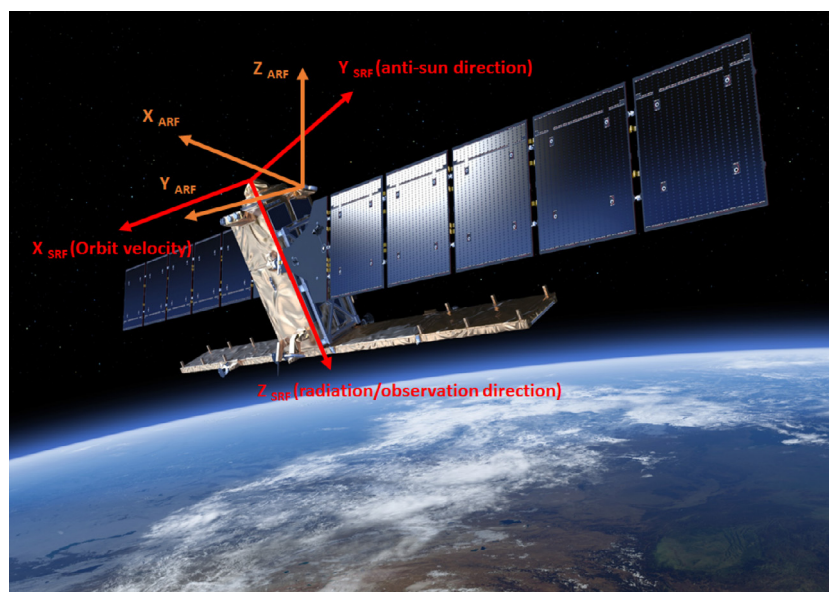

Fig. 1. Artist's impression of the S-1A satellite; copyright: ESA; satellite reference (SRF) and antenna reference frame (ARF) included, see Section 2.

PCVs may induce orbit offsets, which is not intended. Thus the corresponding PCVs are not independent from the POD models and the orbit determination approach used.

Section 2 summarises information on the S-1A mission needed for the GPS data and orbit determination processing. In particular, information necessary for POD is included. Section 3 briefly describes the Copernicus POD Service mainly in view of S-1A. First orbit comparison results are shown in Section 4. Investigations of the systematic orbit offsets are the topic of Section 5. Finally, updated phase center offsets (PCOs) and variations (PCVs) are presented together with new orbit comparison results in Section 6.

2. Information on the Sentinel-1A satellite

Precise orbit determination of a satellite is only possible if precise information is available about the definition of the satellite axes systems and the coordinates of the CoG of the satellite. Additionally, the GPS ARPs and the antenna phase center corrections are needed for POD processing. In order to consider the vector from the antenna phase center to the CoG correctly in the processing the attitude control has to be known as well.

The two relevant satellite axes system on S-1A are the satellite and the antenna reference system (see Fig. 1). The origin of the right-handed satellite reference (SRF) system is the geometric center of the circle defined by the launcher/Spacecraft interface points in the separation plane when the satellite is in stowed launch configuration. The X_{SRF} axis is parallel to the main axis of the SAR antenna, and positive in the direction of the spacecraft velocity vector the spacecraft being in nominal attitude (description follows below). The Z_{SRF} axis is perpendicular to the SAR antenna face direction and positive in direction of radiation. The Y_{SRF} axis completes the right-handed orthogonal coordinate system. It is positive in the direction pointing away from the sun in the nominal operational attitude.

The antenna reference (ARF) system is a right-handed coordinate system as well. The origin of the system is the ARP of the corresponding GPS antenna. The ARF system is rotated with respect to the SRF system by the following angles:

- Roll (X axis): $24.39° + 180° = 204.39°$
- Pitch (Y axis): $14.64°$
- Yaw (Z axis): $0°$

The coordinates of the CoG and the ARPs of the GPS antennas are given in the SRF system and the antenna phase center offsets (PCOs) are given in the ARF system (see Table 1). The mass and the CoG of the satellite change during mission time due to fuel consumption for manoeuvres. The CoG coordinates in Table 1 are the values at the beginning of the mission. The mass of the satellite has been 2158.777 kg.

The nominal attitude mode of the satellite is the Nominal Mission Mode. In Nominal Mission Mode the orbital reference frame is aligned with the Zero-Doppler Orbital Reference Frame (ZDORF). The origin of the ZDORF is the spacecraft's in-flight center of mass. The first axis R is parallel to V, the inertial velocity vector corrected for Earth's rotation, i.e. the Earth-fixed velocity vector. The second axis T is perpendicular to R and defined as $T = R \times P$, where P is the unit vector parallel to the local normal of the Earth's reference ellipsoid (WGS84). The third axis L completes the right-handed frame $L = R \times T$. The nominal attitude of S-1A is composed of two rotations. The rotation from J2000 to ZDORF (Fiedler et al., 2005) and the rotation from ZDORF to the SRF system, the so-called roll steering law. For formulas and parameters of the roll steering law we refer to Miranda (2015).

In-plane and out-of-plane manoeuvres are needed to hold the satellite in a pre-defined orbit tube (GMES, 2004; Martin Serrano et al., 2012). These manoeuvres regularly take place on several days per month. The time, duration and expected thrust are recorded in dedicated manoeuvre files available for the POD processing.

Table 2
Regular Service Review periods and comparison time intervals.

RSR	RSR time period	Orbit comparison interval
1	Oct 2014–Jan 2015	11 Jan–25 Jan 2015
2	Feb 2015–May 2015	28 Mar–11 Apr 2015

Table 1
Coordinates of CoG (Begin of Life) and of the ARPs and PCOs of main and redundant GPS antenna.

	X_{SRF} (m)	Y_{SRF} (m)	Z_{SRF} (m)
CoG	0.0040	−0.0090	2.0050
ARP GPS main	−0.9762	0.2869	0.1241
ARP GPS redundant	−0.9855	0.5135	0.2293
	X_{ARF} (mm)	Y_{ARF} (mm)	Z_{ARF} (mm)
PCOs	−0.5[a]	1.0[a]	97.0[b]

[a] The values for X_{ARF} and Y_{ARF} were exchanged for the results of RSR (Regular Service Review)#1 and #2 presented in Section 4.
[b] Original value is 97.0 mm (used by DLR (Deutsches Zentrum für Luft- und Raumfahrt)). To have PCVs of 0.0 mm in the zenith of the antenna, the CPOD Service adapted the value to 99.5 mm after the generation of the PCVs for the main GPS antenna.

Table 3

Summary of models and parameters employed for the S-1A orbit determination.

CPOD	ESOC	DLR	TUD	AIUB	TUM
NAPEOS	NAPEOS	GHOST	GHOST	Bernese GNSS Software	Bernese GNSS Software
Reference system – IERS Conventions					
2010	2010	2003	2003	2010	2010
GPS measurement model *– ionosphere-free linear combination of undifferenced observations*					
pseudorange/carrier phase noise					
0.8 m/10 mm	1.0 m/10 mm	0.5 m/30 mm	0.5 m/30 mm	–/1 mm (L1&L2)	1 m/10 mm
Antenna phase wind-up					
Applied	Applied	Applied	Applied	Applied	Applied
Sentinel-1A PCOs (mm) $X_{ARF}/Y_{ARF}/Z_{ARF}$, PCVs from					
1.0/−0.5/99.5 GMV	1.0/−0.5/99.5 GMV	1.0/−0.5/97.0 DLR	1.0/−0.5/99.5 GMV	1.0/−0.5/99.5 AIUB	1.0/−0.5/99.5 GMV
GPS final orbit and clock products (clock sampling)					
IGS[a] (30 s)	ESOC (30 s)	CODE[b] (5 s)	IGS (30 s)	CODE (5 s)	CODE (5 s)
GPS antenna PCOs and PCVs from					
igs08.atx[c]	igs08.atx	igs08.atx	igs08.atx	igs08.atx	igs08.atx
Arc length					
72 h	24 h	30 h	30 h	24 h	30 h
Gravitational force models					
Gravity field model (degree × order (static), degree × order (time variable))					
EIGEN-6S2 [d] (120 × 120, 50 × 50)	EIGEN-6S2 (120 × 120, 50 × 50)	EIGEN-GLO4C[e] (120 × 120)	GOCO03S[f] (150 × 150)	EGM2008[g] (120 × 120)	EIGEN-GLO4C (120 × 120)
Ocean tide model (degree × order)					
EOT11a[h] (50 × 50)	EOT11a (50 × 50)	CSR 3.0[i] (30 × 30)	FES2004[j] (50 × 50)	FES2004 (50 × 50)	FES2004 (50 × 50)
Non-gravitational force models					
Atmospheric drag (# of coefficients) – atmosphere density model					
macro model (6/24 h) MSISE90[k]	Constant area (10/24 h) MSISE00[l]	Constant area (1/arc) Jacchia 71 Gill[m]	Constant area (1/arc) Jacchia 71 Gill	– –	Constant area (fixed) MSISE90
Radiation pressure (# of coefficients)					
Macro model (1/arc)	Constant area (fixed)	Constant area (1/arc)	Constant area (1/arc)	–	Constant area (fixed)
Earth albedo radiation (# of coefficients)					
Macro model (fixed)	NAPEOS (fixed)	–	–	–	–
Infrared radiation (# of coefficients)					
Macro model (fixed)	NAPEOS (fixed)	–	–	–	–
Empirical parameters (sets/time or time resolution)					
A, O	A, O	R, A, O	R, A, O	R, A, O Constant (1/24 h)	R, A, O Constant
	Constant				
sin, cos (1/12 h)	sin, cos (1/12 h)				sin, cos (1/24 h)
		Constrained piece-wise constant accelerations (10 min)	Constrained piece-wise constant accelerations (10 min)	Constrained piece-wise constant accelerations (6 min)	constrained stochastic velocity changes (15 min)

[a] International GNSS Service (Dow et al., 2009).

[b] Center for Orbit Determination in Europe (Dach et al., 2016).

[c] Schmid et al. (2016).

[d] Rudenko et al. (2014).

[e] Förste et al. (2008).

[f] Mayer-Gürr et al. (2012).

[g] Pavlis et al. (2012).

[h] Savcenko and Bosch (2012).

[i] Eanes et al. (1995).

[j] Lyard et al. (2006).

[k] Hedin (1991).

[l] Picone et al. (2002).

[m] Jacchia (1971).

The GPS observation unit is provided by RUAG Space. The 8-channel receivers are in principle the same as on the Swarm satellites (Zangerl et al., 2014). The antennas (Öhgren et al., 2011) are slightly different with a new Patch Excited Cup (PEC) element and two choke rings compared to those used on the Swarm satellites.

3. Copernicus POD Service

The Copernicus POD Service is a consortium led by the spanish company GMV. The members of the consortium are

- GMV, Spain
- PosiTim UG, Germany
- Veripos, U.K.
- German Space Operation Center, Deutsches Zentrum für Luft- und Raumfahrt (DLR), Germany
- Institut für Astronomische und Physikalische Geodäsie, Technische Universität München (TUM), Germany
- Astronomical Institute, University of Bern (AIUB), Switzerland
- Faculty of Aerospace Engineering, Delft University of Technology (TUD), The Netherlands

The members have different responsibilities within the CPOD Service. The role and the duties of each member are described in detail in Fernández et al. (2015). The CPOD Service is responsible for the operational POD of the Sentinel-1, -2, and -3 missions. Different orbital products have to be delivered for the different missions, all of them with different latencies and accuracy requirements. In the case of Sentinel-1 two operational POD products are delivered. The near real-time (NRT) orbit product covers two orbital revolutions and has to be delivered with a latency of 3 h. The accuracy requirement for the NRT product is 10 cm in 2D (along-track, out-of-plane). The non-time critical (NTC) orbit product has to be delivered within 20 days and covers 26 h (24 h + 1 h before and after the corresponding day). The NTC accuracy requirement is 5 cm in 3D.

The POD software core of the CPOD Service is NAPEOS, the ESA/ESOC (European Space Agency/European Space Operations Centre) software for precise orbit determination. The three Sentinel missions are very different in terms of latency and accuracy requirements of their orbital products and in terms of the satellite design and properties. In order to facilitate maintenance of the complex CPOD Service system the same core POD setup is used for all three missions to the extent possible. More details on the CPOD Service structure and the setup of the operational processing are given in Fernández et al. (2015).

The Copernicus POD Quality Working Group (QWG) is an integral part of the CPOD Service. The group is chaired by ESA and co-chaired by EUMETSAT (European Organisation for the Exploitation of Meteorological Satellites). Representatives of each Sentinel mission (Mission Processing Centres, Payload Data Ground Segments, and Post-Launch Support) are members of the QWG. Since the launch of Sentinel-3A CNES (Centre Nationales d' Études Spatiales) is also member, because the institute is delivering operational orbits for Sentinel-3.

The core of the QWG are, aside from GMV, five institutions with a long LEO POD expertise, namely AIUB (e.g. Jäggi et al., 2006; Bock et al., 2014), DLR (e.g. Montenbruck et al., 2008), TUD (e.g. Visser et al., 2009; van den IJssel et al., 2015), TUM (e.g. Švehla and Rothacher, 2003), and ESOC (e.g. Flohrer et al., 2011).

4. Orbit determination and comparison results

Orbit solutions delivered by the members of the POD QWG are used for the CPOD NTC orbit validation on a regular basis. Every four months a so-called Regular Service Review (RSR) is performed. Orbit solutions from a selected time interval of about two weeks within the RSR period are compared to each other. Table 2 lists the two RSR periods together with the time intervals actually used for orbit comparison.

4.1. Orbit determination procedures

The orbit solutions from the CPOD Service and from the QWG are all based on the reduced-dynamic orbit determination approach. However, different software packages with different background models, orbit parameterizations, constraints and number of empirical parameters are used. A summary of models and parameters used for the various orbit solutions of RSR#1 and #2 is given in Table 3. The values used for the PCOs, ARPs and CoG are already mentioned in Table 1. Attitude quaternions are not available for the entire orbital revolutions but only during SAR measurements. Due to the incompleteness of the attitude quaternions the attitude is modeled by all groups according to the model described in Section 2. Comparisons to available attitude quaternions confirmed the correct implementation at the different centres. The main differences between the groups are the application of different PCO and PCV combinations and the different usage of dynamical orbit parameters empirical parameters. The two groups using NAPEOS, CPOD and ESOC, apply the most dynamical approach for the S-1A orbit determination. Empirical parameters are only used in along-track and out-of-plane direction and the validity of these parameters is 12 h long. The two groups using GHOST (GPS High Precision Orbit Determination Software Tools, Montenbruck et al., 2005), DLR and TUD, apply models for non-gravitational forces as well. Additionally, constrained piece-wise constant accelerations every 10 min are set up in all three directions as empirical parameters to compensate force model deficiencies. The two remaining groups, AIUB and TUM, use the Bernese GNSS Software (Dach et al., 2015). TUM partly applies non-gravitational force models but

also a large number of empirical parameters are used. AIUB is the only group not applying any non-gravitational force model but only empirical parameters. Especially in radial direction, AIUB and TUM are estimating a constant acceleration for the entire arc of 24 h and 30 h, respectively.

The NAPEOS and GHOST solutions are mainly following the dynamic models (gravitational and non-gravitational) and only a low number of empirical parameters are applied. Inconsistencies in the processing are mainly reflected in the carrier phase residuals. The solutions from the Bernese GNSS Software are close to a kinematic solution, because they use few (TUM) or no (AIUB) non-gravitational force models and many empirical parameters. Mainly the radial leveling of these solutions is driven by the geometry given by the GPS measurements and the satellite information. In this case inconsistencies in the processing are to a large extent absorbed by the empirical parameters. These fundamentally different setups are important to detect inconsistencies in the given satellite geometry.

All groups are applying PCVs in their processing. GMV has provided them from an in-flight calibration (Peter et al., 2015) based on the carrier phase residual approach using ionosphere-free GPS data (Jäggi et al., 2009). AIUB and DLR use their own derived PCV maps, which are based on the carrier phase residual approach as well. GMV and AIUB have both used 11 days of data and they have performed one iteration. DLR has used 36 days of data and three iterations. TUD has improved the GMV PCV map by one iteration in their processing (only for RSR#2).

4.2. Orbit comparison

The orbit solutions are all cut to the central 24 h to harmonise the orbit comparison. Since not all groups deliver orbit solutions on manoeuvre days, these days are excluded from the comparisons. In the RSR #1 comparison interval satellite manoeuvres were carried out on 14, 16, 21, and 22 January 2015 and in the RSR #2 comparison interval on 2 and 9 April 2015.

Fig. 2 shows the results from the comparison of the official CPOD orbits with the orbits from the five QWG institutions for the RSR #1 comparison interval and Fig. 3 shows the corresponding results for the RSR #2 comparison interval. Mean offsets, RMS and standard deviations are displayed independently for the three directions in radial, along-track, and out-of-plane. In the bottom panels the mean 3D RMS values are displayed for the different comparisons. The solution named AIUB(G) is an additional solution from AIUB applying the PCV map from GMV. The largest mean offsets may be observed in the radial direction for the comparison to AIUB (−3.17 cm) and TUM (−1.35 cm) and in out-of-plane direction for the comparison to DLR (2.93 cm) and TUD (2.45 cm). Interestingly, the solution AIUB(G) does not show such

Fig. 2. RSR #1 comparison interval: Mean values (cm) of daily offsets, RMS and standard deviations from comparison between official CPOD orbits and orbits from QWG institutions.

Fig. 3. RSR #2 comparison interval: Mean values (mm) of daily offsets, RMS and standard deviations from comparison between official CPOD orbits and orbits from QWG institutions.

a large radial offset (only −1.35 cm) as the AIUB solution applying the AIUB PCV map. The radial offset of AIUB (G) is the same as the radial offset of TUM with respect to the CPOD orbits. Overall, all comparisons are below the 5 cm in 3D except DLR (6.16 cm).

Table 4 summarises the mean offsets (lower left triangle) and mean standard deviations (top right triangle) for all cross-comparisons (except AIUB(G)) separated into the three directions radial, along-track and out-of-plane for the RSR #1 comparison interval. Mean offsets larger than 3 cm are written in bold numbers. The smallest mean standard deviations from inter-software comparisons are written in italic and are framed.

The radial component of the AIUB orbits shows a significant offset of more than 3 cm to all other orbit solutions except TUM using the Bernese GNSS Software as well. However, the mean standard deviations for inter-software comparisons show the smallest values in radial (1.20 cm) and along-track (1.54 cm) and the second smallest value for the out-of-plane (0.98 cm) component between AIUB and ESOC. Thus these two orbit solutions have a very good consistency despite the large radial offset of −3.16 cm. The consistency is in particular remarkable because of the two different software packages involved and the different set of orbit models and parameters used.

The orbit comparison for the RSR#2 interval (Fig. 3) gives very similar results. The same conclusions as for RSR#1 may be drawn. The AIUB and TUM orbits have

a significant radial offset (−3.22 cm and −2.29 cm, respectively) with respect to the CPOD solution and in the out-of-plane direction DLR and TUD have significant offsets (4.05 cm and 4.44 cm, respectively). The along-track differences are larger than for the RSR#1 test interval. The radial offset of the AIUB(G) solution (−1.44 cm) is again much smaller than for the AIUB solution. The application of different PCVs obviously leads to a different radial leveling of the AIUB orbits, which implies that the PCVs are inducing different radial offsets.

5. Investigations on systematic radial orbit offsets

The analysis of the systematic orbit offsets is focused on the most pronounced discrepancy in the radial direction. Significant offsets in out-of-plane direction are present as well. All groups use empirical parameters for the out-of-plane direction. Therefore, it is not as clear as for the radial direction what the cause of such significant differences could be. The first step is to minimize the differences in radial direction and in future, the discrepancies in out-of-plane direction will be investigated in more detail.

The impact of applying different PCVs for the orbit determination plays an important role for the analysis of the systematic orbit differences in radial direction. Fig. 4 shows the different antenna PCVs (GMV, AIUB, and DLR) for the ionosphere-free linear combination of the carrier phase measurements in an azimuth-elevation map.

Table 4

RSR #1 comparison interval: Mean offsets (lower triangle) and mean standard deviations (upper triangle) (cm); R: radial, A: along-track, O: out-of-plane.

|		CPOD	ESOC	DLR	TUD	AIUB	TUM
					Mean standard deviation		
CPOD	R		0.65	1.99	1.48	1.22	1.37
	A		1.72	4.20	3.38	2.19	2.42
	O		0.74	2.71	1.09	1.12	1.24
ESOC	R	-0.02		1.95	1.35	*1.20*	1.35
	A	0.64		4.01	3.01	*1.54*	1.78
	O	1.58		2.64	0.90	0.98	1.07
DLR	R	0.36	0.38		1.30	2.00	2.20
	A	-0.06	-0.71		2.58	4.06	4.22
	O	2.93	1.34		2.25	2.42	2.59
TUD	R	0.40	0.41	0.03		1.54	1.66
	A	-0.20	-0.84	-0.10		3.10	3.13
	O	2.45	0.87	-0.47		*0.79*	0.86
AIUB	R	**-3.17**	**-3.16**	**-3.53**	**-3.57**		0.92
	A	0.21	-0.43	0.27	0.41		1.38
	O	0.89	-0.69	- 2.04	-1.56		0.99
TUM	R	-1.35	-1.34	-1.72	-1.75	1.82	
	A	0.63	-0.01	0.69	0.83	0.42	
	O	0.17	-1.41	-2.76	-2.28	-0.72	
		Mean offsets					
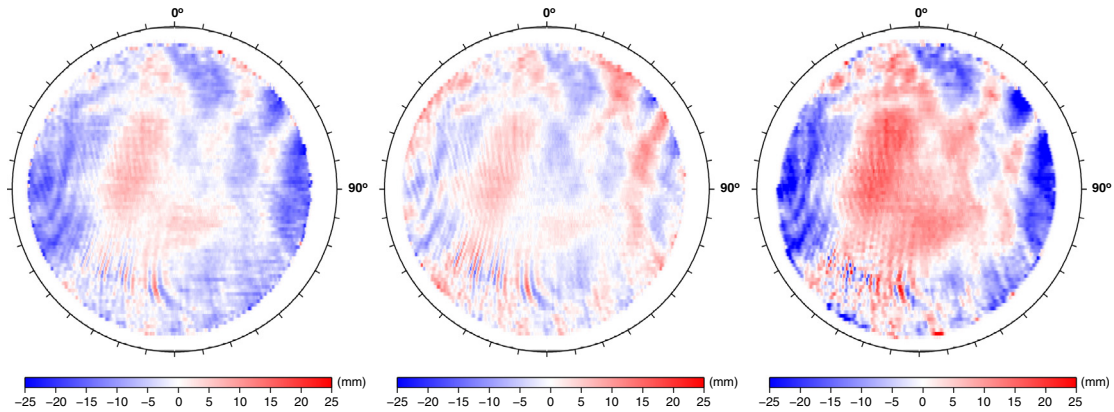
Fig. 4. Azimuth-elevation dependent PCVs (mm, 1° bins) for the main GPS antenna of S-1A used for RSR #1 and #2, flight direction is in azimuth direction of 90°; left: GMV, middle: AIUB, right: DLR.
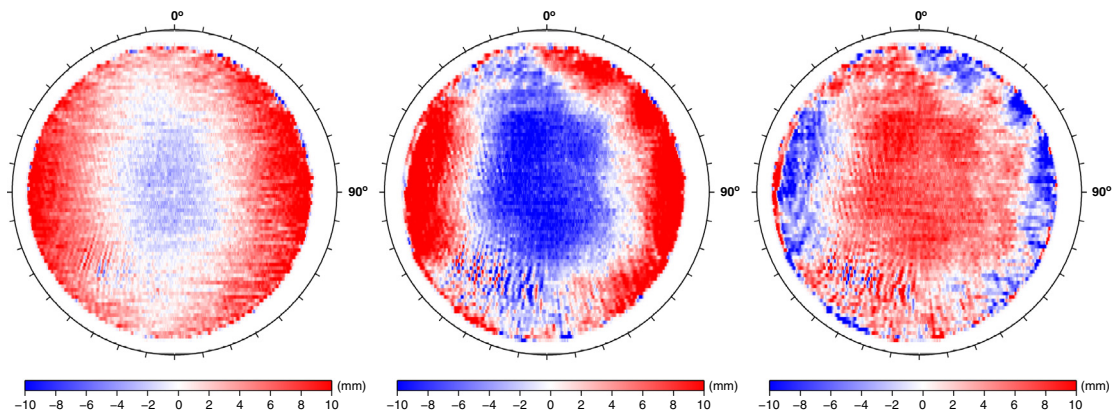

Fig. 5. Differences between S-1A PCVs (mm, 1° bins), left: AIUB-GMV, middle: AIUB-DLR, right: DLR-GMV.

The S-1A flight direction is in azimuth direction of 90°. The main pattern of the PCVs caused by the antenna itself and the satellite environment is similar for all three PCV sets. The differences between the PCVs displayed in Fig. 5 (left: AIUB minus GMV, middle: AIUB minus DLR, right: DLR minus GMV) show, however, significant systematics between the different sets of PCVs.

The systematic differences between the AIUB and GMV PCV are responsible for the different radial leveling of the AIUB orbits. To explain this the interaction between PCOs and PCVs has to be described. According to Rothacher et al. (1995) antenna phase center corrections have some inherent degrees of freedom. A set of antenna phase center corrections consists of a PCO vector $\mathbf{r_0}$ and the PCVs $\phi(\alpha, z)$, being a function of azimuth α and zenith distance z. Such a set is not unique and may be transformed into a new set $\mathbf{r_0'}$ and $\phi'(\alpha, z)$ according to

$$\mathbf{r_0'} = \mathbf{r_0} + \Delta\mathbf{r}$$
$$\phi'(\alpha, z) = \phi(\alpha, z) - \Delta\mathbf{r} \cdot \mathbf{e} + \Delta\phi, \quad (1)$$

where $\Delta\phi$ is an arbitrary offset, which cannot be separated from the receiver clock. The unit vector $\mathbf{e}$ denotes the direction from the receiver to the satellite. The offset vector $\Delta\mathbf{r}$ may be chosen arbitrarily. It is not mandatory but

preferably PCVs should not induce a phase center offset and $\Delta\mathbf{r}$ should be zero. In that case the mean antenna phase center is explicitly defined by the PCOs. This convention is in particular important if one would only apply PCOs and no PCVs.

In order to check for the available S-1A PCVs whether the characteristics may be explained by $\Delta\mathbf{r} \neq 0$ a least squares adjustment is set up. The vector $\Delta\mathbf{r} = (E, N, U)$ and $\Delta\phi$ are the unknowns, which are determined from the given PCVs $\phi'(\alpha, z)$. With $\mathbf{e} = (\sin\alpha \cdot \sin z, \cos\alpha \cdot \sin z, \cos z)$ PCVs may be expressed as follows

$$\phi'(\alpha, z) = -\sin\alpha \cdot \sin z \cdot E - \cos\alpha \cdot \sin z \cdot N - \cos z \cdot U + \Delta\phi$$
$$(2)$$

If the estimated parameters E, N, and U are different from zero the given PCVs are inducing a phase center offset. In practice, it has to be considered that according to Jäggi et al. (2009) carrier phase ambiguities absorb a mean signal in the PCVs, which take effect along the satellite passes within the GPS antenna frame (Fig. 2 in Jäggi et al., 2009). In the case of S-1A the nominal flight direction corresponds to an azimuth angle of 90° in the antenna frame. In a simplified model the segments between azimuth

angles of $135°$ and $225°, 315°$ and $360°$, and $0°$ and $45°$ are affected from this absorption by the carrier phase ambiguities for S-1A.

The various PCVs used for the S-1A orbit determination (see Fig. 4) are checked for induced offsets by estimating them according to the least squares adjustment based on Eq. (2). The specific azimuth regions mentioned before are excluded and only the bins populated by observations on a specific day (11 January 2015) are considered for the estimation of the offsets. Table 5 summarises the resulting offsets. The most right column lists the a posteriori RMS values $\tilde{\Omega}$ of the corresponding least squares adjustment.

The values of $\Delta\phi$ may be ignored, because they cannot be separated from the receiver clocks. The values for E and N are small for all three PCVs. The U value for the AIUB PCVs is very small as well. Only the values for U from the GMV (-1.75 cm) and DLR (-3.19 cm) PCVs are significantly larger than all other values.

In nominal attitude of S-1A the U direction of the GPS antenna approximately corresponds to the radial orbit direction. The AIUB(G) orbits are shifted by 1.82 cm in radial direction with respect to the AIUB orbits for RSR#1 (mean radial offset AIUB(G) $\leftrightarrow$ CPOD: -1.35 cm; AIUB $\leftrightarrow$ CPOD: -3.17 cm) and 1.78 cm for RSR#2 (-1.44 cm and -3.22 cm). In average the systematic radial orbit difference between the two different AIUB orbit solutions is 1.80 cm, which is very close to the estimated GMV U offset of 1.75 cm.

The AIUB(G) and also the TUM solutions fully include the U offset induced by the GMV PCVs. The AIUB solutions do not include this offset. Due to the empirical and free parametrization the reduced-dynamic orbit determination approach used at AIUB and TUM is very close to a kinematic-like orbit determination. The radial leveling of the AIUB, AIUB(G) and TUM orbits is fully given by the geometry of the GPS observations including the offsets induced by the used PCVs (from AIUB or GMV) and the geometry given from the satellite, such as GPS antenna location with respect to the CoG. Inconsistencies in the processing are absorbed by the unconstrained empirical accelerations in radial direction being constant over the entire orbital arc.

In the case of CPOD (DLR, ESOC, and TUD), the radial leveling of the orbit is fixed by the force models acting partly or fully in the radial direction (e.g., solar radiation pressure, Earth albedo radiation, infrared radiation). No (or heavily constrained) empirical parameters are set up in radial direction. Thus, any erroneous information

about the satellite and antenna geometry in radial direction cannot be absorbed by any parameter directly effective in radial direction but is mainly reflected in the carrier phase observation residuals. The residuals were, however, used for the in-flight calibration of the PCVs and the U offset maps into the PCVs. The U offset induced by the GMV (and DLR) PCVs and the large systematic radial orbit offset of the kinematic-like solutions AIUB and TUM are, therefore, an indicator for an inconsistency between models and geometry. It may be assumed that non-perfect non-gravitational force models are not able to shift the orbit significantly in radial direction. To confirm this assumption an orbit determination run is done with NAPEOS switching off all non-gravitational models. The resulting orbit is compared to an orbit with the modeling applied for CPOD as mentioned in Table 3. The orbit comparison revealed a systematic radial orbit difference of only 3.7 mm. This means that the application of neither an erroneous nor no non-gravitational force model is able to shift the orbit more than a few mm in radial direction.

It may be noticed that the induced U offset of the DLR PCVs (-3.19 cm) is much larger than the one of the GMV PCVs (-1.75 cm). The DLR PCV offset is very close to the observed mean radial differences between AIUB and CPOD (-3.17 cm), ESOC (-3.16 cm), DLR (-3.53 cm), and TUD (-3.53 cm). This may be explained by the number of iterations used for the determination of the PCVs. GMV has done only one iteration whereas DLR has performed three iterations. Many studies have shown that several iterations are needed for a reliable PCV generation (Jäggi et al., 2009; Bock et al., 2011; van den IJssel et al., 2015). In this case also several iterations were needed to get a good approximation of the full radial inconsistency in the PCVs. The conclusion is that an erroneous information of approximately 3 cm is given in the satellite (CoG coordinates) or antenna geometry (antenna offsets and PCOs). Since no other observation technique is available for an independent validation it cannot be further distinguished where the inconsistency comes from.

One way of determining the correct geometry would be to estimate the vector between CoG and antenna phase center in the SRF system directly within a fully dynamic orbit determination procedure. In principle, this is possible when applying a dynamic orbit determination without estimating empirical parameters. In the case of S-1A this vector is not aligned to the radial, along-track, and out-of-plane directions of the orbit due to the rotation of the GPS antenna with respect to the satellite body and due to the nominal attitude control (see Section 2). The antenna offset estimation in NAPEOS is only possible along the directions of the SRF system. Therefore, all components of the offset vector would have to be set up to get the corrected offset in radial direction. The estimation of an offset in along-track direction (corresponding to X_{SRF}) is, however, fully correlated to the receiver clock correction estimates. The offset vector estimation is, therefore, currently not possible for S-1A.

Table 5
Estimated induced offsets from different PCVs.

PCVs from	E (cm)	N (cm)	**U (cm)**	$\Delta\phi$ (cm)	$\tilde{\Omega}$ (cm)
GMV	0.14	0.13	**−1.75**	−1.46	0.37
AIUB	0.01	0.11	**−0.15**	−0.08	0.36
DLR	0.12	0.38	**−3.19**	−2.17	0.58

Bold: Values for U approximately correspond to radial direction.

In addition, the least squares adjustment described in Eq. (2) to estimate the offsets induced by PCVs can easily be used for this purpose. The correct geometry may be found by estimating the offsets from PCVs, which are generated based on different geometry.

Several PCVs are generated based on the data of the comparison interval from RSR#1. For each set of PCVs the U resp. Z_{ARF} value of the PCOs is changed. The E resp. X_{ARF} and N resp. Y_{ARF} values are fixed to the pre-launch values in Table 1. The resulting PCVs are then tested by estimating the induced offsets. The specific azimuth regions already mentioned earlier are excluded and only the bins populated by observations on 11 January 2015 are used for the estimation. Table 6 summarises the corresponding estimated values. With $U_{upd} = 68$ mm no radial offset is induced by the PCVs. The resulting U-value is 29 mm smaller than the original value of 97 mm and 31.5 mm smaller than the value of 99.5 mm, which was used together with the first PCV map from GMV. The difference of 31.5 mm coincides very well to the observed radial orbit differences

Table 6
Estimated induced offsets from different PCVs when using various values as U_{upd}.

U_{upd} (mm)	E' (mm)	N' (mm)	U' (mm)	$\tilde{\Omega}$ (mm)
97.0	1.84	1.36	−18.06	4.42
47.0	−1.63	1.31	13.08	4.19
57.0	−0.92	1.32	6.84	4.15
67.0	−0.24	1.33	0.63	4.15
68.0	**−0.17**	**1.33**	**0.00**	**4.15**

Bold: Best fitting values.

Table 7
Updated PCOs for main and redundant GPS antenna.

	X_{ARF} (mm)	Y_{ARF} (mm)	Z_{ARF} (mm)
PCOs	−0.5	1.0	68.0

between AIUB and the other groups (except TUM) for RSR#1 and #2.

6. Updated PCOs and PCVs for Sentinel-1A GPS antennas

Table 7 lists the new PCOs, which were used to generate a new set of PCVs for the main GPS antenna for S-1A. The new set of PCVs has been generated by PosiTim in five iterations based on 256 days of data. Fig. 6 (left) shows the new PCVs for the main GPS antenna in an azimuth-elevation map. As expected the main systematics within the antenna frame are still the same as in the first PCV map (Fig. 4 (left)). Due to the large amount of data used for the estimation the new map is smoother than the first map. The estimated induced offsets are now −0.76, 0.84, 0.32 mm for E', N', U', respectively. All three values are below 1 mm indicating that the updated PCVs should not induce significant offsets when being used in a kinematic-like orbit determination. Fig. 6(right) shows the PCVs for the redundant GPS antenna. The PCVs have been generated from 28 days of data distributed over July, August, and September 2015 when the redundant GPS unit was running instead of the main GPS unit. First orbit comparisons for days with data based on the redundant GPS unit revealed the same systematic radial offset as for the main GPS unit. Therefore, the PCVs are also generated based on the updated PCO values listed in Table 7. The resulting induced offsets are 0.23, −0.80, 2.71 mm for E', N', U', respectively.

A reprocessing of the entire year 2015 has been done from the QWG members to have a long-term series available for comparison. The sets of updated PCOs (Table 7) and PCVs for the two antennas (Fig. 6) are used from CPOD, ESOC, DLR, TUD, and TUM. AIUB has done six iterations to generate new PCVs for the main (59 days of data) and for the redundant (36 days of data) GPS antennas based on the updated PCOs. The following additional model and parametrization updates are done from
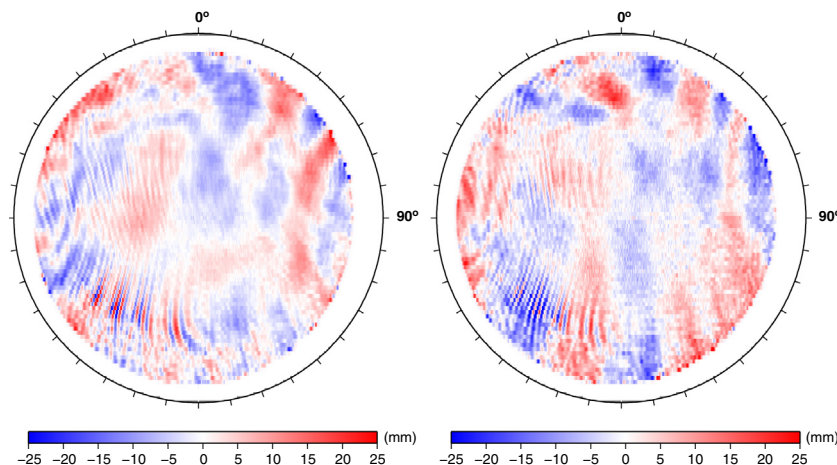

Fig. 6. Azimuth-elevation map of new PCVs (mm) for S-1A; left: main GPS antenna based on 256 days of data; right: redundant GPS antenna based on 28 days of data; flight direction is in azimuth direction of 90°.

Table 8
RSR #1 comparison interval after PCO/PCV update: Mean offsets (lower triangle) and mean standard deviations (upper triangle) (cm).

		CPOD	ESOC	DLR	TUD	AIUB	TUM
					Mean standard deviation		
CPOD	R		0.72	0.86	0.82	1.26	1.33
	A		1.26	1.64	1.60	1.96	2.09
	O		0.60	1.08	0.95	1.12	1.16
ESOC	R	0.04		0.78	0.68	0.89	1.10
	A	0.29		1.44	1.40	1.53	1.79
	O	1.04		1.10	0.97	1.18	1.19
DLR	R	0.05	0.01		0.31	0.78	1.01
	A	0.27	-0.02		0.63	0.97	1.31
	O	0.68	-0.36		0.52	0.50	0.91
TUD	R	-0.32	0.29	0.27		0.75	0.95
	A	-0.33	0.04	0.06		1.07	1.37
	O	-0.82	-0.23	0.13		0.64	0.78
AIUB	R	0.46	0.43	0.41	0.14		0.90
	A	0.53	0.24	0.26	0.20		1.22
	O	1.07	0.03	0.39	0.26		0.93
TUM	R	-0.06	0.02	0.01	-0.26	-0.40	
	A	0.15	-0.44	-0.42	-0.48	-0.68	
	O	-1.36	0.32	0.68	0.55	0.29	
		Mean offsets					
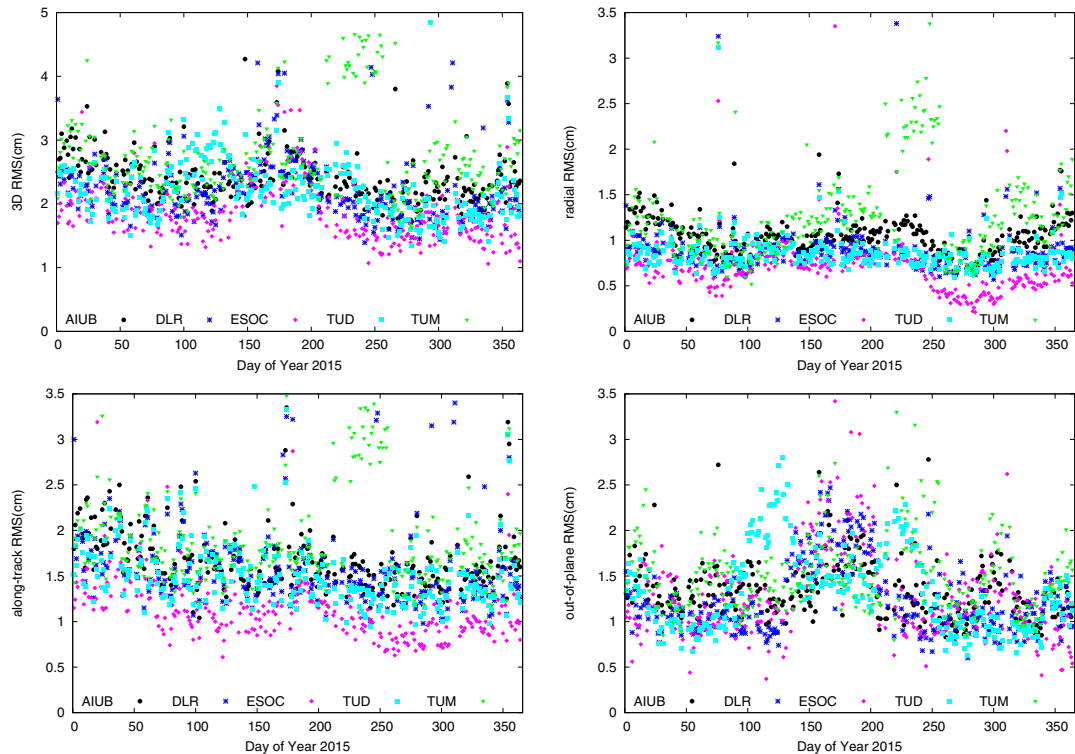
Fig. 7. Reprocessed year 2015, RMS values (cm) of comparison between re-processed CPOD orbits and orbits from QWG members.
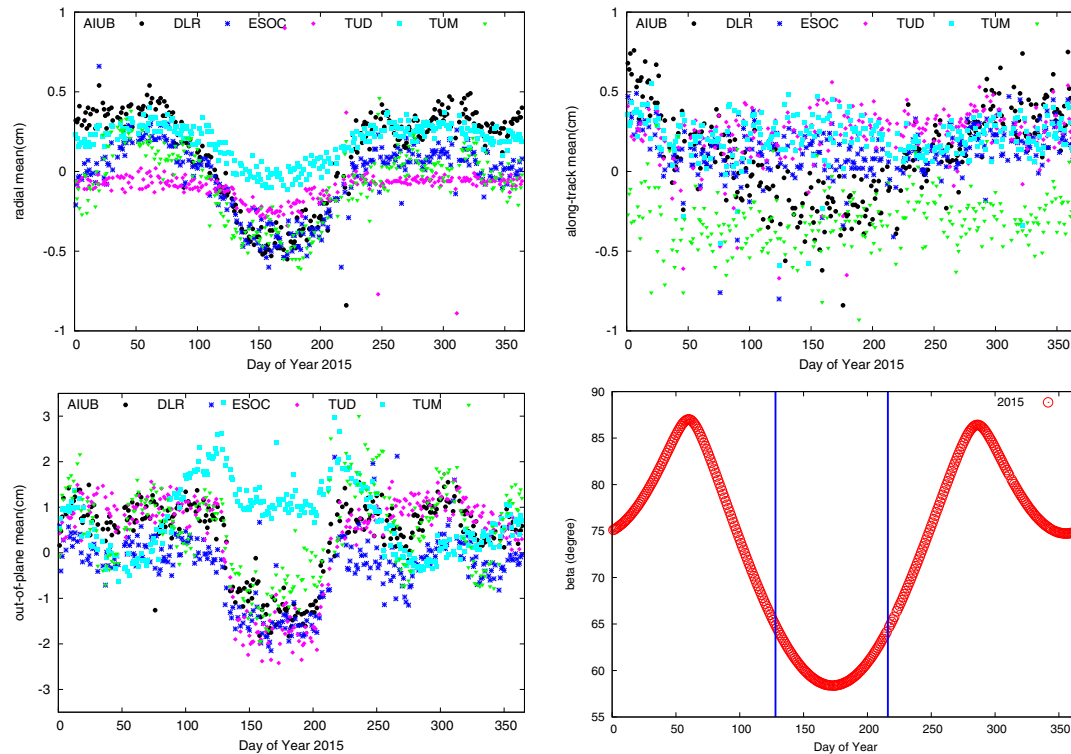
Fig. 8. Reprocessed year 2015, Mean offset values (cm) of comparison between re-processed CPOD orbits and orbits from QWG members; bottom right: Sun elevation angle over the orbital plane of S-1A, vertical lines show the eclipse period in the middle of the year.

the different groups for the reprocessed orbit solutions (AIUB und TUM did no further changes):

- CPOD: Arc length shortening from 72 h to 48 h and update of the satellite macro model
- ESOC: switch to macro model for surface modeling
- DLR: Improved observation weighting ratio pseudorange/carrier phase measurements (0.5/0.03m to 0.6/0.007m) and major software update from GHOST 2.0 to GHOST 2.1 with the following changes:
  - gravity field model: EIGEN-GL04C (120 × 120) → GOCO03S (100 × 100)
  - surface model: cannon-ball → macro model
  - atmospheric density model: Jacchia 71 Gill → NRLMSISE-00
  - IERS conventions: 2003 → 2010
  - Earth radiation: no → CERES-ES4 (Wielicki et al., 1996), macro model
- TUD: observation weighting ratio pseudorange/carrier phase measurements is changed from 0.5/0.03 m to 0.6/0.006 m

To have a direct comparison to the solutions from Section 4 Table 8 presents the updated mean offsets and standard deviations for the RSR#1 comparison interval in January 2015. The corresponding mean 3D RMS values for the comparison of the updated orbit solutions are for ESOC 1.95 cm, DLR 2.30 cm, TUD 2.28 cm, AIUB 2.91 cm and TUM 3.12 cm. These values are well below

the 5 cm limit and it can directly be noted from the values in Table 8 that the large mean radial offsets could be removed. The largest mean radial offset of only 0.46 cm is observed between AIUB and CPOD. This confirms that the modification of the PCO Up offset from 97 mm to 68 mm removed the geometry inconsistency to a large extent. The mean standard deviations also significantly decreased showing the largest value of 2.09 cm for the along-track comparison between CPOD and TUM. The smallest mean standard deviations from inter-software comparisons (italic and framed) are now ESOC vers. TUD with 0.68 cm in radial direction and DLR vers. AIUB with 0.97 cm and 0.50 cm in along-track and out-of-plane direction, respectively. These are remarkably small numbers. The improvement of the standard deviations reflects the orbit modeling improvements made by the different groups.

The comparison between the reprocessed CPOD and each other reprocessed orbits from the QWG members is done for the entire year 2015. Fig. 7 shows the daily 3D (top left), radial (top right), along-track (bottom left), and out-of-plane (bottom right) RMS values of these comparisons. The scale of the y-axis of the 3D RMS plot (5 cm) is different to the other three plots (3.5 cm). Most of the orbit solutions compare to the CPOD orbits between 1 and 3 cm 3D RMS (65 manoeuvre days are excluded from the comparison). The mean 3D RMS values over the entire year are all well within 5 cm with ESOC 1.90 cm, DLR 2.42 cm, TUD 2.34 cm, AIUB 2.47 cm and TUM 2.83 cm. The cloud of points larger than 4 cm 3D RMS

between days 209 and 257 for TUM are the days where the redundant receiver was running instead of the main receiver. Although the setup has carefully been checked the reason for the worse TUM solutions is not clear.

Beside that the orbit solutions are all very close together. Mainly in out-of-plane direction seasonal variations are present, which can also be seen in the daily mean offset values displayed in Fig. 8. Variations may also be noticed for the radial mean offsets but it has to be noted that the scale of the panel with the out-of-plane mean offsets (bottom left) is larger than for the panels with the radial (top left) and along-track (top right) mean offsets. The bottom right panel illustrates the angle of the Sun over the S-1A orbit plane. The vertical lines indicate the eclipse period in the middle of the year. It is obvious that the seasonal variations in the mean radial and out-of-plane offsets are correlated with the Sun elevation angle and the eclipse period. Mainly for AIUB and TUM the mean radial offsets are much smaller as for the first solutions but there are still variations of up to ±5 mm over the year for all solutions compared to CPOD. The cause is not yet clear. It might be inaccurate macro models of the satellite, not-optimized parametrization in the orbit modeling or still a satellite geometry inconsistency. The setup of all groups have to be checked and optimised. Further investigations and comparisons are needed to minimize the differences furthermore. The same statement holds for the cause of the large amplitude and variation of the mean out-of-plane offsets.

Nevertheless, the long-term orbit comparison shows the very good consistency of all six orbit solutions, independent from the software package and orbit parametrization used. The orbit solutions compare all well within the required 5 cm 3D RMS although these comparisons cannot give an absolute orbit accuracy.

7. Conclusion

The Copernicus POD Service is responsible for the precise orbit determination of the C-Band SAR satellite Sentinel-1A, the first satellite of the European Copernicus programme. The service is supported by the Copernicus POD Quality Working Group delivering five independent orbit solutions for the validation of the GPS-derived Sentinel-1A orbit products. First orbit comparisons revealed a systematic radial offset between various orbit solutions of about 3 cm. Due to the different parametrization and orbit models used for the orbit determination by the different groups, this systematic orbit offset could be identified as an erroneous information in the satellite geometry. The magnitude of the inconsistency (29 mm) could be confirmed by a least squares adjustment, which allows to estimate phase center offsets induced by PCVs.

Based on the corrected geometry a long-term comparison for the entire year 2015 has been performed and the consistency between the six orbit solutions is well within the required orbit accuracy of 5 cm in 3D RMS. In princi-

ple, the comparison of only GPS-derived orbits cannot give an absolute orbit accuracy. However, due to the different – from more dynamic to kinematic-like – reduced-dynamic orbit determination approaches used, the orbit comparison may deliver very good indication of the final orbit accuracy.

Investigations are still needed in the future to further minimise remaining seasonal variations in the orbit differences mainly being obvious during the eclipse period of the satellite.

References

Aschbacher, J., Milagro-Pérez, M., 2012. The European Earth monitoring GMES programme: status and perspectives. Remote Sens. Environ. 120, 3–8. http://dx.doi.org/10.1016/j.rse.2011.08.028.

Bock, H., Jäggi, A., Meyer, U., et al., 2011. Impact of GPS antenna phase center variations on precise orbits of the GOCE satellite. Adv. Space Res. 47 (11), 1885–1893. http://dx.doi.org/10.1016/j.asr.2011.01.017.

Bock, H., Jäggi, A., Beutler, G., et al., 2014. GOCE: precise orbit determination for the entire mission. J. Geod. 88 (11), 1047–1060. http://dx.doi.org/10.1007/s00190-014-0742-8.

Dach, R., Schaer, S., Arnold, D., et al., 2016. CODE Final Product Series for the IGS. Published by Astronomical Institute, University of Bern. http://dx.doi.org/10.7892/boris.75876. <http://www.aiub.unibe.ch/download/CODE>.

Dach, R., Lutz, S., Walser, P., et al. (Eds.), 2015, Bernese GNSS Software Version 5.2. University of Bern, Bern Open Publishing. ISBN: 978-3-906813-05-9. http://dx.doi.org/10.7892/boris.72297.

Dow, J.M., Neilan, R.E., Rizos, C., 2009. The international GNSS service in a changing landscape of global navigation satellite systems. J. Geod. 83 (3–4), 191–198. http://dx.doi.org/10.1007/s00190-008-0300-3.

Eanes, R.J., Bettadpur, S., 1995. The CSR 3.0 Global Ocean Tide Model: Diurnal and Semi-diurnal Ocean Tides from TOPEX/Poseidon Altimetry. Technical Memorandum, Center for Space Research, CSR-TM-95-06.

Fernández, J., Escobar, D., Águeda, F., et al., 2014. Sentinels POD service operations. In: SpaceOps 2014 Conference, SpaceOps Conferences, AIAA 2014-1929. http://dx.doi.org/10.2514/6.2014-1929.

Fernández, J., Escobar, D., Ayuga, F., et al., 2015. Copernicus POD service operations. In: Proceedings of the Sentinel-3 for Science Workshop, 2–5 June 2015, Venice, Italy

Fiedler, H., Börner, E., Mittermayer, J., et al., 2005. Total zero doppler steering – a new method for minimizing the doppler centroid. IEEE – Geosci. Remote Sens. Lett. 2 (2), 141–145. http://dx.doi.org/10.1109/LGRS.2005.844591.

Fletcher, K. (Ed.), 2012. Sentinel-1: ESAs Radar Observatory Mission for GMES Operational Services, ESA SP-1322/1. ESA Communications. ISBN 978-92-9221-418-0.

Flohrer, C., Otten, M., Springer, T., et al., 2011. Generating precise and homogeneous orbits for Jason-1 and Jason-2. Adv. Space Res. 48 (1), 152–172. http://dx.doi.org/10.1016/j.asr.2011.02.017.

Förste, C., Schmidt, R., Stubenvoll, R., et al., 2008. The GFZ/GRGS satellite-only and combined gravity field models: EIGEN-GLO4S1 and EIGEN-GLO4C. J. Geod. 82 (6), 331–346. http://dx.doi.org/10.1007/s00190-007-0183-8.

GMES Sentinel-1 Team, GMES Sentinel-1 System Requirements Document, ES-RS-ESA-SY-0001. <http://emits.sso.esa.int/emits-doc/ESTEC/4782-annex-a.pdf>.

Hedin, A.E., 1991. Extension of the MSIS thermosphere model into the middle and lower atmosphere. J. Geophys. Res. 96 (A2), 1159–1172. http://dx.doi.org/10.1029/90JA02125.

Jacchia, L.G., 1971. Revised Static Models of the Thermosphere and Exosphere with Empirical Temperature Profiles. SAO Special Report 332, Cambridge.

Jäggi, A., Dach, R., Montenbruck, O., et al., 2009. Phase center modeling for LEO GPS receiver antennas and its impact on precise orbit determination. J. Geod. 83 (12), 1145–1162. http://dx.doi.org/10.1007/s00190-009-0333-2.

Jäggi, A., Hugentobler, U., Beutler, G., 2006. Pseudo-stochastic orbit modeling techniques for low-Earth orbiters. J. Geod. 80 (1), 47–60. http://dx.doi.org/10.1007/s00190-006-0029-9.

Loiselet, M., Stricker, N., Menard, Y., et al., 2000. GRAS-MetOp's GPS-based atmospheric sounder. ESA Bull. 102, 38–44.

Lyard, F., Lefevre, F., Letellier, T., et al., 2006. Modelling the global ocean tides: modern insights from FES2004. Ocean Dyn. 56, 394–415. http://dx.doi.org/10.1007/s10236-006-0086-x.

Martin Serrano, M.A., Shurmer, I., Marc, X., 2012. Sentinel-1: operational approach to the orbit control strategy. In: Proceedings 23th International Symposium on Space Flight Dynamics – 23th ISSFD, Pasadena, US.

Mayer-Gürr, T., Rieser, D., Hoeck, E., et al., 2012. The new combined satellite only model GOCO03S. Presentation at International Symposium on Gravity, Geoid and Height Systems GGHS2012, Venice, Italy, October 9–12, 2012.

McCarthy, D.D., Petit, G., 2004. IERS Conventions (IERS Technical Note 32). Frankfurt am Main: Verlag des Bundesamts für Kartographie und Geodäsie, 127 pp. Paperback. ISBN 3-89888-884-3 (print version).

Miranda, N., 2015. Sentinel-1 Instrument Processing Facility. Technical Note, ESA-EOPG-CSCOP-TN-0004. <https://sentinel.esa.int/documents/247904/1653440/Sentinel-1-IPF_EAP_Phase_correction>.

Montenbruck, O., van Hellepute, T., Kroes, R., et al., 2005. Reduced dynamic orbit determination using GPS code and carrier measurements. Aerosp. Sci. Technol. 9 (3), 261–271. http://dx.doi.org/10.1016/j.ast.2005.01.003.

Montenbruck, O., Andres, Y., Bock, H., et al., 2008. Tracking and orbit determination performance of the GRAS instrument on MetOp-A. GPS Solut. 12 (4), 289–299. http://dx.doi.org/10.1007/s10291-008-0091-2.

Öhgren, M., Bonnedal, M., Ingvarson, P., 2011. GNSS antenna for precise orbit determination including S/C interference predictions. In: Proceedings of the 5th European Conference on Antennas and Propagation (EUCAP), 11–15 April, 2011, Rome, Italy, 1990–1994.

Pavlis, N.K., Holmes, S.A., Kenyon, S.C., et al., 2012. The development and evolution of the Earth Gravitational Model 2008 (EGM2008). J. Geophys. Res. 117 (B4). http://dx.doi.org/10.1029/2011JB008916.

Peter, H., Springer, T., Otten, M., et al., 2015. Supporting the copernicus POD service. In: Proceedings of the Sentinel-3 for Science Workshop, 2–5 June 2015, Venice, Italy.

Petit, G., Luzum, B., 2010. IERS Conventions (IERS Technical Note 36). Frankfurt am Main: Verlag des Bundesamts für Kartographie und Geodäsie, 179 pp. Paperback. ISBN 3-89888-989-6 (print version).

Picone, J.M., Hedin, A.E., Drob, D.P., et al., 2002. NRLMSISE-00 empirical model of the atmosphere: statistical comparisons and scientific issues. J. Geophys. Res. 107 (A12). http://dx.doi.org/10.1029/2002JA009430, SIA 15-1–SIA 15-6.

Rothacher, M., Schaer S., Mervart, L., et al., 1995. Determination of antenna phase center variations using GPS data. In: Proceedings of the IGS Workshop 1995, Potsdam, Germany. <http://kb.igs.org/hc/en-us/articles/202112016-Workshop-1995-proceedings.

Rudenko, S., Dettmering, D., Esselborn, S., et al., 2014. Influence of time variable geopotential models on precise orbits of altimetry satellites, global and regional mean sea level trends. Adv. Space Res. 54 (1), 92–118. http://dx.doi.org/10.1016/j.asr.2014.03.010.

Savcenko, R., Bosch, W., 2012. EOT11A – Empirical Ocean Tide Model from Mulit-Mission Satellite Altimetry. DGFI Report No. 89, München, Deutsches Geodätisches Forschungsinstitut.

Schmid, R., Dach, R., Collilieux, X., et al., 2016. Absolute IGS antenna phase center model igs08.atx: status and potential improvements. J. Geod. 90 (4), 343–364. http://dx.doi.org/10.1007/s00190-015-0876-3.

Springer, T., Dilssner, F., Escobar, D., 2011. NAPEOS: The ESA/ESOC Tool for Space Geodesy.

Švehla, D., Rothacher, M., 2003. Kinematic and reduced-dynamic precise orbit determination of low Earth orbiters. Adv. Geosci. 1, 47–56. http://dx.doi.org/10.5914/adgeo-1-47-2003.

Torres, R., Snoeij, P., Geudtner, D., et al., 2012. GMES Sentinel-1 mission. Remote Sens. Environ. 120, 9–24. http://dx.doi.org/10.1016/j.rse.2011.05.028.

van den IJssel, J., Encarnação, J., Doornbos, E., et al., 2015. Precise science orbits for the Swarm satellite constellation. Adv. Space Res. 56 (6), 1042–1055. http://dx.doi.org/10.1016/j.asr.2015.06.002.

Visser, P., van den IJssel, J., van Hellepute, T., et al., 2009. Orbit determination for the GOCE satellite. Adv. Space Res. 43 (5), 760–768. http://dx.doi.org/10.1016/j.asr.2008.09.016.

Wielicki, B.A., Barkstrom, B.R., Harrison, E.F., et al., 1996. Clouds and the Earth's Radiant Energy System (CERES): an earth observing system experiment. Bull. Am. Meteorol. Soc. 77, 853–868.

Wu, S.C., Yunck, T.P., Thornton, C.L., 1991. Reduced-dynamic technique for precise orbit determination of low Earth satellites. J. Guid. Control Dyn. 14 (1), 24–30. http://dx.doi.org/10.2514/3.20600.

Zangerl, F., Griesauer, F., Sust, M., et al., 2014. SWARM GPS precise orbit determination receiver initial in-orbit performance evaluation. In: Proceedings of ION-GNSS+-2014, 10–12 Sept 2014, Tampa, FL, USA.